



# Influence of column position on stability of stiffened deep mixed column-supported embankment over soft clay

Zhen Zhang<sup>1</sup> · Guangyao Li<sup>1</sup> · Guan-Bao Ye<sup>1</sup> · Meng Wang<sup>2</sup> · Yan Xiao<sup>3</sup> · Tianxiong Chen<sup>4</sup>

Received: 14 August 2022 / Accepted: 7 May 2023 / Published online: 12 June 2023  
© The Author(s), under exclusive licence to Springer-Verlag GmbH Germany, part of Springer Nature 2023

## Abstract

When stiffened deep mixed (SDM) columns are used to support embankments over soft soil, the embankment stability becomes one of the major concerns for geotechnical engineers. However, limit studies have been focused on failure of SDM columns under embankment load. This paper conducted a series of scale-reduced model tests to investigate stability of embankment over soft soils with SDM columns, including columns installed under the embankment base, and columns installed only under the embankment crest and the embankment side slope, respectively. A load system consisting of six loading plates was designed to create a uniform surcharge on the embankment crest. An aluminum foil tape was implanted into each core pile in a row to detect the model column failure during surcharge loading, as its electric resistance becomes infinity when the tape was broken due to the rupture of column. With the increase in the surcharge, the failure mode and process of SDM column were analyzed based on the peak stress on the top of column and strain difference along column length and the electric resistance change of aluminum foil tape. The test results showed that the SDM columns under the embankment crest also had effects on enhancing the embankment stability, even though the slip plane may not pass through them. With the increase in surcharge, the SDM columns failed progressively and had possible failure under compression, a combination of compression and bending, and bending depending on locations of the columns under embankment. The progressive failure mechanism was discussed.

**Keywords** Embankment · Model test · Progressive failure · Stability · Stiffened deep mixed column

## 1 Introduction

Stiffened deep mixed (SDM) column consisting of a central core pile and an outer deep mixed (DM) column is formed by inserting a rigid column (e.g., plain concrete,

reinforced concrete, or a spun pile) into the center of DM column before its hardening [27]. Due to the existence of core pile, SDM column has a significantly greater stiffness and strength than conventional deep DM column [24]. This technique has been successfully adopted to improve soft

---

✉ Guan-Bao Ye  
guanbaoye@gmail.com  
Zhen Zhang  
zhenzhang@tongji.edu.cn  
Guangyao Li  
2032255@tongji.edu.cn  
Meng Wang  
meng\_wang2@arcplus.com.cn  
Yan Xiao  
513331034@qq.com  
Tianxiong Chen  
chentx@kundeyt.com

<sup>1</sup> Key Laboratory of Geotechnical and Underground Engineering of Ministry of Education, Department of Geotechnical Engineering, Tongji University, Shanghai 200092, China  
<sup>2</sup> East China Architectural Design & Research Institute Co., Ltd, Shanghai 200011, China  
<sup>3</sup> Guangzhou City Construction & Development Co. Ltd., Guangdong 510030, China  
<sup>4</sup> ZheJiang Kunde Innovate Geotechnical Engineering Co., Ltd., Ningbo 315000, Zhejiang, China

soils in roadways, railways and building structures around the world [4].

When columns are used to support embankments over soft soil, engineers may have concerns over bearing capacity and settlement of subsoil, and embankment stability. Dong et al. [3] indicated that SDM column can remarkably reduce the vertical displacement of foundation as compared with DM column, and the improvement became significant as the length of core pile increased. Voottipruex et al. [18] stated that the bearing capacity of a single SDM column was 3–3.6 times that of a conventional DM column with the same column geometry. Gao et al. [4] confirmed this improvement factor on vertical bearing capacity from practical application. Jamsawang et al. [5] found that the horizontal bearing capacity of SDM column was 11–15 times that of the DM column with the same size. Wonglert et al. [19] found that there were three possible failure modes for a SDM column under vertical load, i.e., soil failure, cement-soil failure at the core pile tip and cement-soil failure at the top of SDM column. Zhang et al. [26] recommended a length ratio (i.e., the ratio of core pile length to DM column length) in range of 0.5–0.8 for sufficiently transferring embankment load to SDM columns. Most past studies were mainly focused on the performance of SDM column under working condition and failure of single column under vertical or lateral force.

Embankment load poses additional horizontal earth pressure in soil, and it transfers between columns and surrounding soils with differential settlement. Thus, columns may have failure modes under embankment different from a single column under a vertical load [9, 10, 13, 29]. Navin et al. [14] and Zhang et al. [25] illustrated that DM columns might fail under shear, bending, rotation and tension depending on locations of the columns under embankment. Bending failure is the possible failure mode for rigid and semi-rigid columns under embankment side slope [1, 15, 22, 28]. Compared with individual column failure, progressive failure is equally important in embankment instability failure [12]. Due to the significant differences in mechanical behaviors between stiffened core pile and outer DM column, the failure of SDM columns under embankment load would be more complex. Thus, the failure of SDM columns under embankment loading is necessary to be investigated. In addition, some calculation methods were developed for analyzing the stability of column-supported embankment [8, 10–12]. Kitazume et al. [10] proposed a stability calculation method considering the collapse failure of the relative rigid column under the side slope of embankment. Kitazume et al. [11] further proposed a stability calculation by assuming that all DM columns under the side slope fail at the same time in bending failure mode. Liyanaphairana et al. [12] proposed an analytical equation to calculate the safety factor of

embankment, assuming that the columns passing through the slip surface reach their shear strength. It can be noted that these calculation methods only consider the contributions of the columns within the slip plane to stability. The contributions of the columns outside the slip plane are still not clear.

This study conducted scale-reduced model tests of SDM column-supported embankment over soft soils under 1 g gravity field. It includes one model test without columns and three model test with SDM columns. Six loading plates, which were connected to six parallel jacks, were placed on the embankment crest to apply a surcharge similar to flexible load on the embankment crest. The progressive failure of SDM column was monitored with the increase in surcharge loading. The failure modes of column at different positions were revealed, and the effect of positions of SDM column under the embankment on the stability of embankment was discussed.

## 2 Model test apparatus and materials

### 2.1 Test apparatus

A series of scale-reduced model tests were conducted to investigate the instability of SDM column-supported embankment over soft soil. The sizes of model embankments were designed at a scale ratio of 1:15 to a typical prototype size. The main components of the test apparatus included a test box, loading frame and load system. Figure 1 illustrates the schematic of the model test. The model box with inside dimensions of 3000 mm long, 990 mm wide and 1800 mm high, was made of steel plates in three sides. The front side of the box was made of toughened glass to allow visual observation and photogrammetry of the embankment during the test. The model box was reinforced by steel frames to minimize its lateral deformations. To minimize the side effect due to the friction of the steel side wall of the box, two layers of polytetrafluoroethylene (PTFE) membrane of 1.0 mm thick were placed on the inside of the steel side walls.

The traffic load on the embankment crest was close to a flexible load. To simulate such surcharge, a loading system was designed consisting of six loading plates, each of which was 125 mm wide and 985 mm long. To obtain the plane strain condition, the length of the loading plate was almost equal to the width of the model box. Each loading plate was connected to a jack, and the jacks were connected in parallel to a hydraulic pump, so that the applied pressure on each loading plate was consistent in magnitude. The hydraulic jack was controlled automatically by computer.

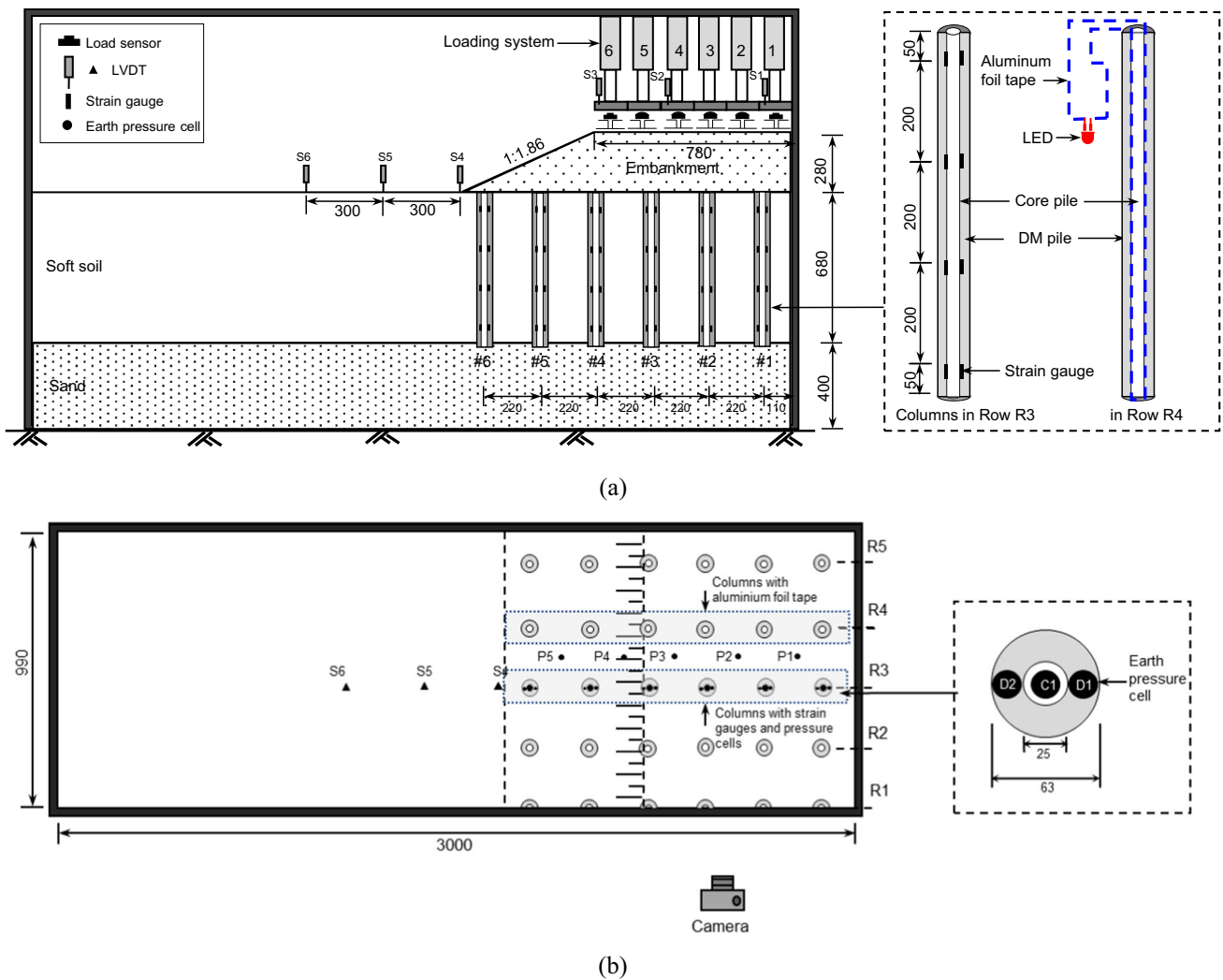


Fig. 1 Schematic of the model test apparatus **a** plan view; **b** cross section (unit: mm)

## 2.2 Model column

Outer column was made of cement-stabilized soil, and core pile was often made of concrete in practice. Considering the scale ratio of 1:15, this study adopted a mixture of gypsum, kaolin, barite, water and glycerol with mass ratio of 0.2:0.9:0.8:0.2 to produce outer column, and the core pile was made of gypsum, quartz sand, water and glycerin with mass ratio of 1:1:5:1:0.2. The quartz sand of 200 mesh (0.075 mm) was used. The mixtures for outer column and core pile were produced into a cubic with dimensions of 70.7 mm × 70.7 mm × 70.7 mm. The cubic specimens were stored in a standard curing room (i.e., at room temperature  $25 \pm 1$  °C and humidity greater than 95%) for the specified curing periods (i.e., 1, 3, 5, 7 and 10 days). The unconfined compressive test was conducted. The results showed that the model materials for outer column and core pile had constant unconfined compressive strengths from 5

to 10 days. During this period, the model materials for outer column and core pile had average unconfined compressive strengths of 0.08 MPa (at a corresponding axial strain of 1.7%) and 2.0 MPa (at a corresponding axial strain of 0.15%), respectively. These properties followed the scale ratio of 1:15 to a typical prototype size, as in practice, and SDM columns have the outer deep mixed columns and concrete core piles with unconfined compressive strengths typically in ranges of 0.4 to 2.0 MPa, and 30 to 35 MPa, respectively [3, 6].

There are three types of SDM columns in practice according the difference in length between DM column and stiffened core pile, namely, the stiffened core pile has a length equal to, shorter or longer than the DM column, depending on the geotechnical conditions and the improvement requirement [18, 19, 21]. When the subsoil consists of a relatively thin soft soil layer underlain by a firm soil, SDM column with equal length of core pile is

commonly adopted. In the model test, a sand soil layer was beneath the soft soil; as a result, the model SDM column with equal length of core pile was adopted. The model core pile and outer column had 25 mm and 63 mm in diameter, respectively, and they both had a length of 700 mm. The ratio of the cross sectional area of the core pile to that of the SDM column was 0.16, which was within the typical ranges of 0.1–0.4 used in the field [32]. A plexiglass tube of 25 mm in inner diameter and 700 mm long was used to manufacture the core pile. The plexiglass tube consisted of two splits, and the inner side wall of the tube was smeared with a thin layer of Vaseline. The prepared mixture for core pile was poured into the tube in three lifts as the tube was placed on a shaking table for removing air bubbles and air pockets. When the tube was filled up, the top of the tube was smoothed by a knife and capped with a plastic film. The model core pile was cured for 24 h. under natural condition before demolding.

The model SDM column was produced using a plexiglass tube of 63 mm in inner diameter and 700 mm long, which also consisted of two splits. The inner side wall of the tube was smeared with a thin layer of Vaseline before producing model column. The manufactured core pile was fixed at the center of the tube, and then, the prepared mixture for the outer column was poured into the tube until to the top of the tube. After filling up the tube, it was placed on a shaking table for removing air bubbles and air pockets. The top of the tube was smoothed and capped with a plastic film. The model SDM column was cured for 24 h. before removing the tube.

The half model columns (the model columns with cross section of semicircle), which were installed at the front side of the model box as shown in Fig. 1, were produced following the similar procedures. When producing the half SDM column, a split tube was placed horizontally, and the both ends were capped with a plastic film. The prepared mixture for the outer column filled up the split tube and left for 10 min. until the mixture reached a certain viscosity. Then, a produced half core pile was pressed into the mixture.

Uniaxial compression test and three-point bending beam test were conducted to test the engineering behavior of the model column. The peak compression strength of the model column was 316.7 kPa at the corresponding axial strain of 0.2%. The maximum moment at the mid-span of the model column was 2.5 N m determined by the center-point flexural test.

### 2.3 Model soils

The model ground consisted of two layers, namely 400-mm-thick sand layer and 680-mm-thick soft soil. The sand layer was made of well-graded river sand. The mean

grain size ( $D_{50}$ ) was 1.9 mm. The uniformity coefficient ( $C_u$ ) and the coefficient of curvature ( $C_c$ ) of the sand were 5.12 and 1.81, respectively. The maximum and minimum dry unit density of the sand were 1.76 g/cm<sup>3</sup> and 1.49 g/cm<sup>3</sup>, respectively. The target relative density of the sand layer was 70%, which was achieved by compaction with fixed mass of sand into a precalculated volume of each lift. The peak friction angle of the sand at the target density was 41° based on the triaxial tests.

The model soft soil was made of a mixture of quartz sand, EPS particles and glycerol. The quartz sand was almost round shape and had particle distribution of 1 to 2 mm. The EPS particles were within the particle distribution of 0.5 to 1.5 mm. The quartz sand, EPS particles and glycerol were mixed with a volume ratio of 1:1:0.03. The maximum and minimum unit density of the model soft soil were 0.78 g/cm<sup>3</sup> and 0.52 g/cm<sup>3</sup>, respectively. The target relative density of the soft soil layer was 50%. The model soil at 50% relatively density had a friction angle of 24°, cohesion of 1.4 kPa and compression modulus of 0.2 MPa.

### 2.4 Model embankment preparation

The model embankment was constructed using quartz sand. The maximum and minimum dry unit density of the sand were 1.58 g/cm<sup>3</sup> and 1.23 g/cm<sup>3</sup>, respectively. The target relative density of the embankment fill was 70%. The model embankment fill at 70% relatively density had a friction angle of 34° based on the triaxial tests.

Table 1 shows the properties of the model materials and their typical properties to the field size. For the most concerned properties (e.g., the strength of outer column and core pile, the strength and modulus of soft soil), their corresponding properties in field size are also included. It can be seen that they almost followed the similarity criterion with scale ratio of 1:15 to a typical prototype size.

## 3 Model test program

### 3.1 Test plan

As shown in Fig. 1, half embankment was designed due to the symmetry of the embankment. To minimize the boundary effect and achieve the plane strain condition, five rows of columns notated as R1–R5 were arranged in the longitudinal direction, in which the row R1 was the half columns, and the rows of R2–R5 were complete columns. The front side of the model box involved half columns, so that the development of slip surface in the SDM column-improved soft soil under embankment can be observed during the test. The columns in the transversal direction

**Table 1** Properties of model material

Items	Properties
Outer column	$q_u = 0.08/1.2$ MPa, $\varepsilon = 1.7/2.7\%$ , $E = 8.5/127.5$ MPa
Core pile	$q_u = 2.0/30.0$ MPa, $\varepsilon = 0.15/0.15\%$ , $E = 1.8/27$ GPa
Sand	$E_s = 16.2$ MPa, $\varphi = 41/41^\circ$ , $\rho = 1.67$ g/cm <sup>3</sup>
Soft soil	$E_s = 0.2/3.0$ MPa, $\varphi = 24/24^\circ$ , $c = 0.6/9.0$ kPa, $\rho = 0.63$ g/cm <sup>3</sup>
Embankment	$E_s = 9.1$ MPa, $\varphi = 34/34^\circ$ , $\rho = 1.58$ g/cm <sup>3</sup>

$q_u$  = unconfined compressive strength;  $\varepsilon$  = corresponding strain at unconfined compressive strength;  $E$  = elastic modulus;  $E_s$  = modulus of compressibility;  $\varphi$  = internal frictional angle;  $c$  = cohesive forces;  $\rho$  = density. A/B, A represents the value in the model scale, and B represents the corresponding value in prototype scale

were notated as #1 to #6 from the embankment centerline to the toe.

To investigate the influence of SDM column position on the embankment stability, this study conducted four model tests, as shown in Fig. 2 and Table 2: (a) one test without columns (notated as T1), which was designed for a comparison purpose; (b) one with columns installed under the embankment base (notate as T2); (c) one with columns only under the embankment crest (notated as T3); and (d) one with columns only under the embankment side slope (notated as T4).

### 3.2 Monitoring instruments

Figure 1 also shows the layout of the monitoring instruments in the model test, including earth pressure cells, linear variable differential transformers (LVDTs), load sensors and strain gauges. Five earth pressure cells were placed at midspan in the surrounding soil, and three earth

**Table 2** Test program

Test label	Outer column		Core pile		Column No
	Diameter/mm	Length/mm	Diameter/mm	Length/mm	
T1	N/A	N/A	N/A	N/A	N/A
T2	63	700	25	700	#1 to #6
T3	63	700	25	700	#4 to #6
T4	63	700	25	700	#1 to #3

pressure cells were installed on the top of each column in row R3, including one on the top of the core pile and two on the top of the outer column, as shown in Fig. 1b. The LVDTs were installed on the loading plates and the ground surface outside the embankment toe to measure the settlement of the embankment and the heaves of the ground. The strain gauges were pasted along the length of each core pile in row R3 at distances of 50 mm, 250 mm, 450 mm and 650 mm away from the column head, and each depth had two strain gauges as shown in Fig. 1a. The load sensors were installed directly under the No.1 and No.6 jacks. A camera was fixed in the front side of the model box, which was used to photograph the cross section of the model during the test. The Geo-PIV technique [17] was used to analyze the slip plane of the SDM column-supported embankment.

To monitor the column failure during the test, this study adopted ultra-thin double-sided conductive aluminum foil tape which was 3 mm wide and 0.06 mm thick. The aluminum foil tape was implanted into each core pile in row R4 to form a conductive path, and a light-emitting diode (LED) was connected in the conductive path for each core pile as shown in Fig. 1a. The aluminum foil tape is flexible,

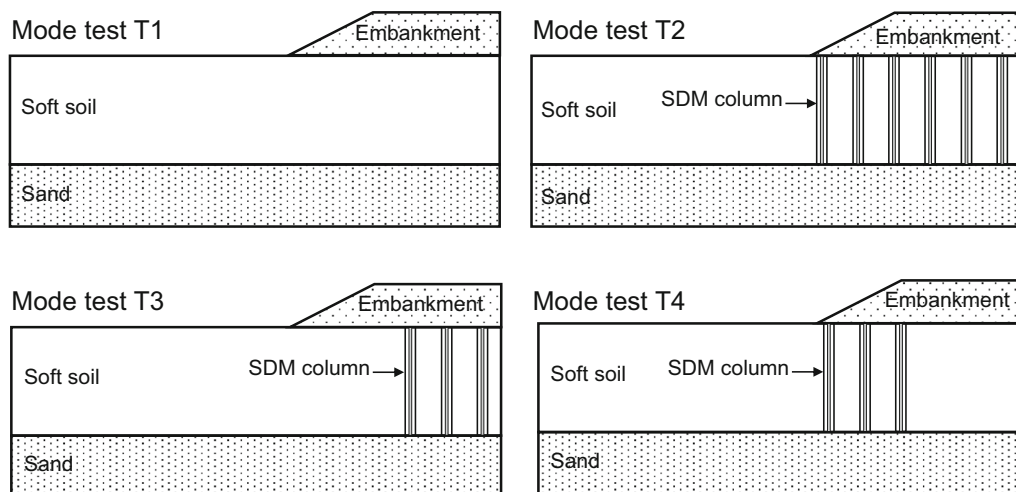


**Fig. 2** Test plans of the model test

and it is easy to be broken by tension. All the LEDs were on when the surcharge was started to apply. When a LED was off at a certain load, it can be an indicator that the column represented by the LED could be broken. The sequence of the LED going off can be used to reflect the sequence of the column failure during the test.

It should be noted that the wires of strain gauges and aluminum foil tapes would be broken by stretching during the test as the surcharge was applied until the instability of model embankment. Thus, the wires were collected together and gone through the bottom of the soft soil layer.

### 3.3 Test procedures

The model test followed the following procedures:

- The model box was prepared, and two layers of PTFE membrane were placed on the inside of the steel side walls.
- During backfilling, the prepared sand was poured into the model box and compacted to a desired lift thickness of 100 mm. In each lift, the soil density was carefully controlled by the mass and volume. The sand layer was compacted to a relative density of 70% (i.e., 1.67 g/cm<sup>3</sup>). After that, the column positions on the top of sand layer were marked, and the model columns were installed with the column tips embedded 20 mm into the sand layer. Laser was used to ensure the verticality of the columns during installation. The wires for connecting strain gauges and aluminum foil tapes were run downwards to the top surface of the sand layer first and then, out of the model box to avoid the rupture of wire during embankment instability. The model soft soil was filled into the model box with a lift of 100 mm thick and carefully compacted to a relative density of 50% using rubber hammer. This procedure was repeated until to the desired thickness of 700 mm.
- Mini-cone penetrometer test was conducted to examine the shear strength of the soft clay [2]. Figure 3 shows the profiles of the shear strength of the soft clay with depth for all test cases. The model soft soil had an internal frictional angle of 24° and a cohesion of 0.6 kPa. As a result, the shear strength of the soft clay in all model tests increased with depth and was almost consistent in all tests. The mini-cone penetrometer test verified the repeatability of the manufactured soft soil.
- The earth pressure cells were installed on the embankment base. The model embankment with a slope of 1.86H:1 V was compacted in each lift of 40 mm until to 280 mm high.

- After the embankment construction was completed, the loading plates were directly placed on the embankment crest with a 5 mm gap between each other, and each plate was connected to the corresponding jack.
- The LVDTs and camera were installed at the designated positions.
- The loading system started up at a rate of 3.5 kPa/sec. until the embankment failed.

## 4 Test results and analyses

### 4.1 Displacement vs. surcharge

Figure 4 shows the variations of the measured displacements with the applied surcharge in all model tests. The model tests behaved a similar regulation, irrespective of the differences in magnitude in each test. When the surcharge was small, the settlements at different positions on the embankment crest were almost same and increased linearly, but the ground outside the embankment heaved at different rate (i.e., the measuring point closer to the embankment increased faster). However, when the applied surcharge exceeded a certain magnitude, the settlements at the positions near the embankment shoulder became larger relatively to that at the embankment certain. Meanwhile, the ground heaved outside the embankment became significant. The soil displacement characteristics are similar to the findings of the rigid column-supported embankment as did by Yu et al. [22].

Based on the curves shown in Fig. 4, the threshold surcharges for accelerating the displacements were 40 kPa,

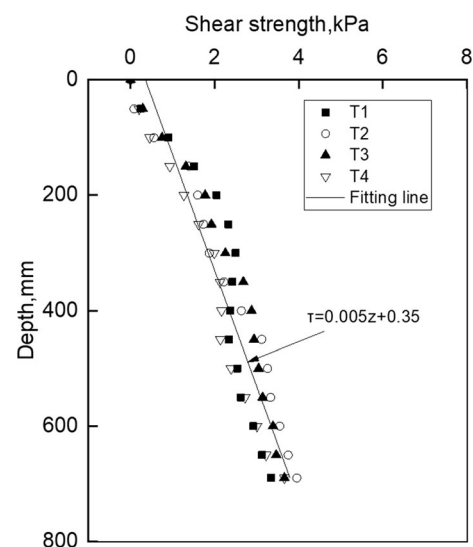
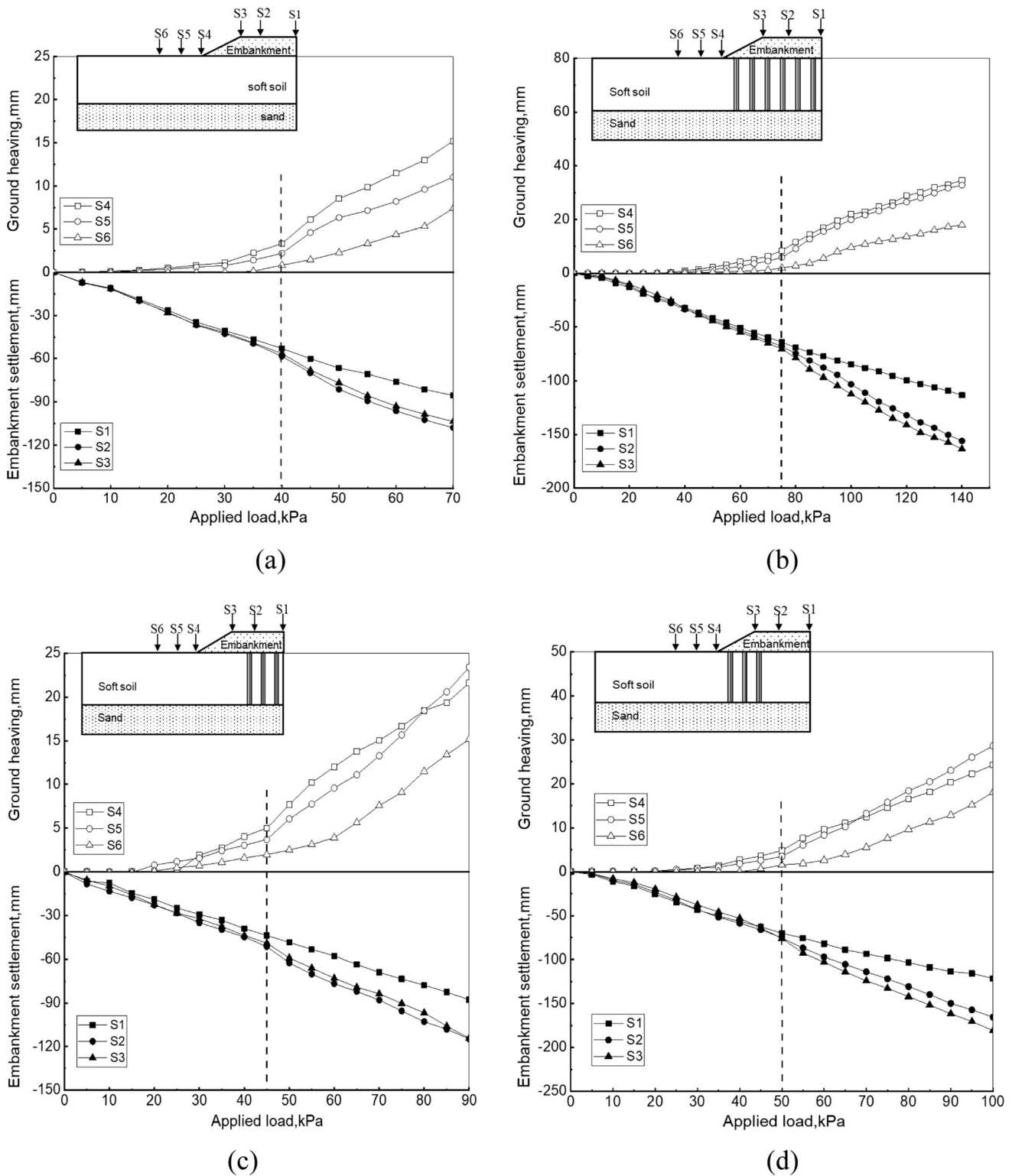


Fig. 3 Variation of shear strength of model ground with depth



**Fig. 4** The displacement changes of experimental groups with the increase in applied load: **a** T1; **b** T2; **c** T3; **d** T4

75 kPa, 45 kPa and 50 kPa in the model tests T1–T4, respectively. As compared to the model test T1, the surcharge increments for the mode tests T2–T4 were 35 kPa, 5 kPa and 10 kPa, respectively. The model test T3 had

slight enhancement on the embankment stability as no columns were installed under the side slope of the embankment. Meanwhile, it is interesting to note that for the mode test T4, its enhancement on the stability was

obviously less than the model test T2, although they both had the columns under the side slope of the embankment. It can be indicated that the columns under the embankment crest and the side slope, both had effects on enhancing the embankment stability.

As shown in Fig. 4c, d, before threshold surcharges for accelerating the displacements, the settlements measured by S1 to S3 increased almost with a same rate. When the surcharge exceeded the threshold surcharge (i.e., the embankment started to fail), the settlement by S2 became larger than that by S3 in Fig. 4c, and the settlement by S3 become larger than that by S1 in Fig. 4d even the monitoring positions of S2 and S3 were above the part of model reinforced by columns. As shown in Fig. 11, S2 was near the slip surface (Fig. 11c), and S3 was inside the sliding zone (Fig. 11d); thus, the instability of embankment resulted in a relatively large settlements of S2 and S3 as compared with those by S3 (Fig. 11c) and S1 (Fig. 11d).

To further investigate the effect of column positions on the embankment stability, the displacements under surcharge of 45 kPa were selected, which was corresponding to the load when the development of displacement became significant in the test T1. As shown in Fig. 5, the settlement of the embankment significantly reduced when the columns were installed under the embankment crest, and the ground heaves evidently reduced when the column was installed under the side slope of the embankment. Moreover, the model test T2 had less settlements on the embankment crest than the model test T3, and less ground heaves outside the embankment than the model test T4. The test results show that installation of columns under the embankment crest not only reduced the embankment settlement, but also had effect on further mitigating the ground heaves.

## 4.2 Vertical stresses on column head

Figure 6 shows the variation of the stresses on the column heads. The stress on the outer column head was the average of the two measured values. Some measurements on certain columns were missing due to the malfunction of earth pressure cells. The columns #1 to #4 had peak stresses of 90–120 kPa on the outer column head and 300 kPa to 370 kPa on the core pile head; however, the columns #5 and #6 had peak stresses less than 10 kPa. In the model test T2, the SDM columns #1 to #4 reached their peak strengths earlier than the threshold stress, while in the model tests T3 and T4, the SDM columns #1 to #4 reached their peak strengths close to or after the threshold stress. In other words, when the embankment stated to fail under the surcharge in the model tests T3 and T4, those SDM columns under the embankment crest had not fully reached vertical bearing capacity.

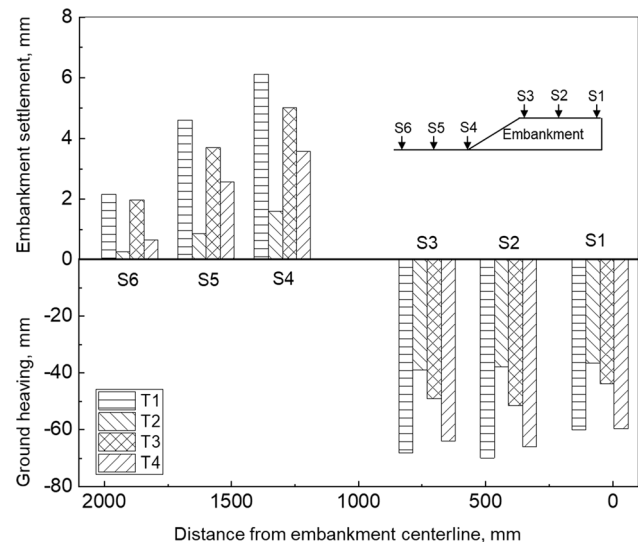


Fig. 5 Displacements of monitoring points under surcharge of 45 kPa

To further assess the load transfer of surcharge onto the embankment base, a stress ratio of the stress on the top of column or surrounding soil to the applied surcharge is determined. Figure 7 shows the stress ratio on the column head and soft soil in the three groups. The stress ratios of columns #2 and #4 in the three groups increased to a peak and then, gradually decreased to a residual value, and the core piles had higher peak stress ratio than the outer column, indicating that more surcharge was concentrated onto the core piles. Furthermore, the surcharges corresponding to the peak stress ratio of outer column were in a range of 15–60 kPa, which are generally smaller than the surcharges corresponding to the peak stress ratio of core pile (i.e., 55 to 65 kPa). In the residual stage, the stress ratios of outer column of columns #2 and #4 approached the stress ratio of the soil at the corresponding locations, while the stress ratios of core pile of columns #2 and #4 were still higher than unity. The column #5 yielded stress ratio less than unity, indicating that this column had minor effect on bearing the vertical stress.

Based on the above analyses, it is evident that the columns #1 to #4 especially the core pile played a prominent role in bearing the vertical load, while the columns #5 and #6 hardly carried vertical load. For the columns #1 to #4, the surcharge would be further concentrated onto the core pile as the outer column yielded earlier than the core pile.

## 4.3 Strains along core pile

There were two strain gauges pasted at the same depth of a core pile in this study. The strain difference, which is determined by the strain at a depth closer to the embankment centerline subtracting that at the same depth on the opposite side of the core pile, is used to examine the



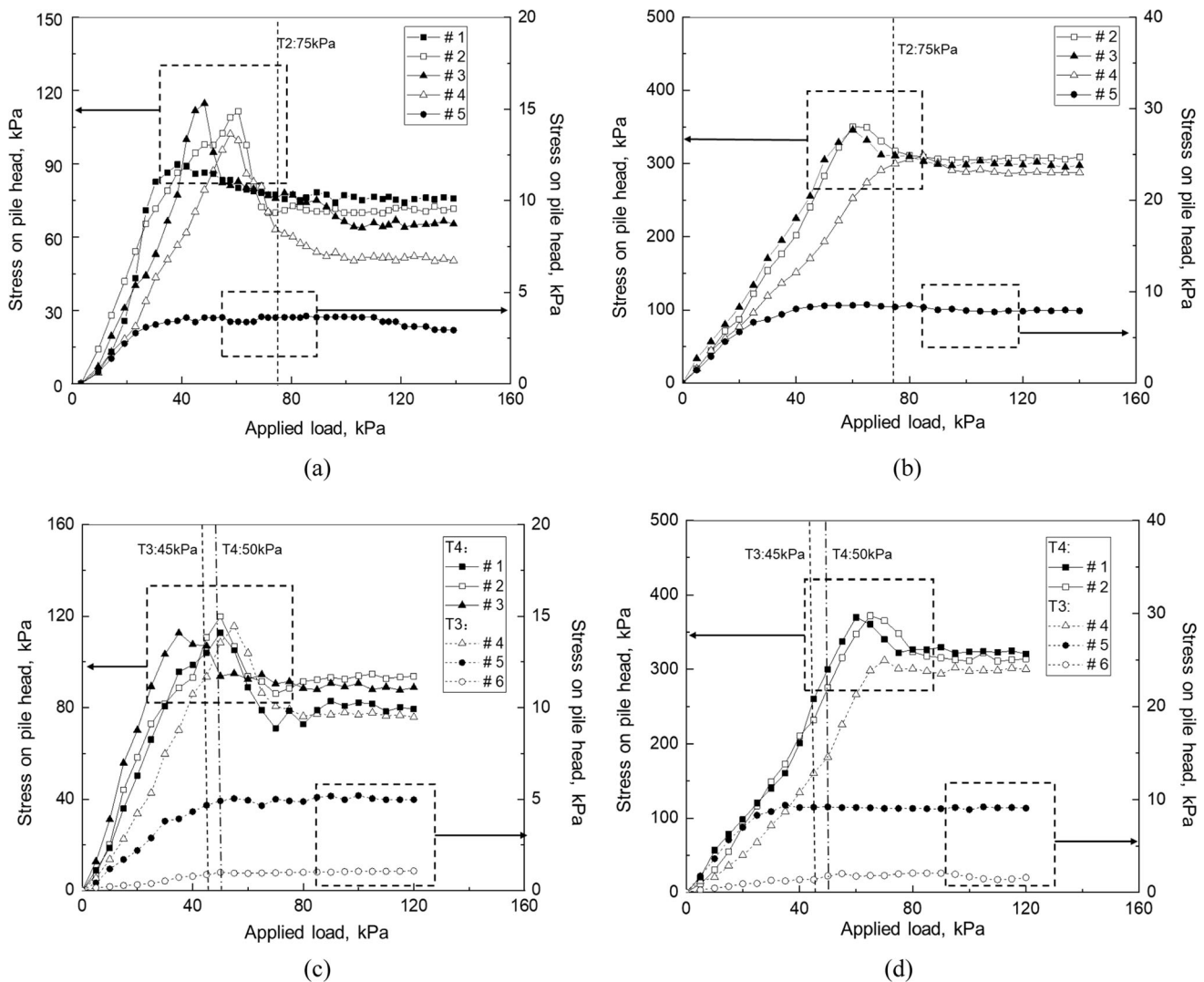


**Fig. 6** Vertical stress of column head: **a** outer columns in T2; **b** core piles in T2; **c** outer columns in T3 and T4; **d** core piles in T3 and T4

mechanical behavior of column, as shown in Fig. 8. The larger strain difference at a depth of core pile indicates a relatively larger bending moment carried by the core pile. The column #3 in the model tests T2 and T3 had small strain differences at each depth, indicating that the column #3 carried less bending moment during the test. The columns #4 to #6 in the model tests T2 and T4 had relatively large strain differences at certain depths, indicating that they all carried relatively large bending moments. Figure 8 also shows that as compared with the corresponding columns in the test T2, the columns 4# to 6# in the test T4 generally had large strain differences at the same depths, even had opposite values. The existence of the columns under the embankment crest influenced the bending movement carried by the columns under the side slope of embankment.

To further investigate the bending behavior of the SDM columns under embankment, the bending moments along

the length of the columns #3 to #6 under the embankment surcharges of 40 kPa, 60 kPa and 80 kPa were calculated, respectively. Fig. 9 shows the distribution of bending moment along core pile, including the bending capacity (i.e.,  $M_{ult}$ ) of the model column determined by the center-point flexural test. The column #3 in the model test T2 and T3 both bore small bending moments. In the model tests T2 and T4, the columns #4 to #6 were subjected to relatively large bending moments at some depths, and some positions approached or exceeded its bending capacity determined by the center-point flexural test. However, the columns #5 and #6 bent in opposite direction. The existence of the columns under the embankment crest influenced the bending mode of the columns under the side slope of embankment. Previous studies indicated that rigid column and DCM column have a possible failure mode by bending under embankment side slope [7, 30, 31].

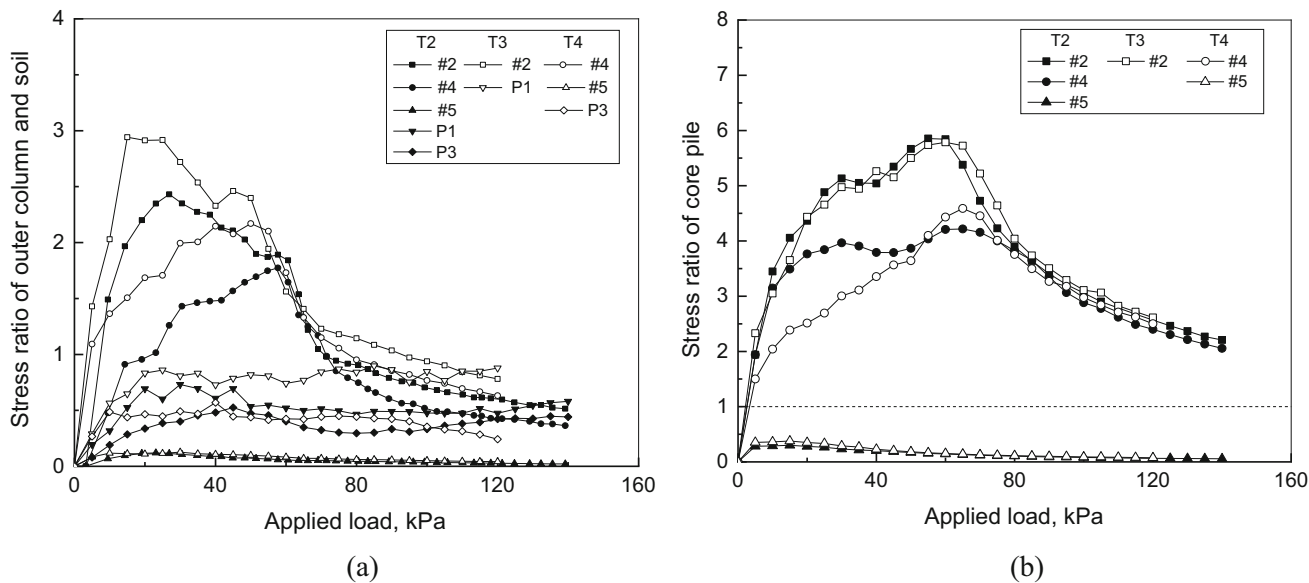


Fig. 7 Stress ratio of column head and soft soil: a outer columns and soil; b core piles

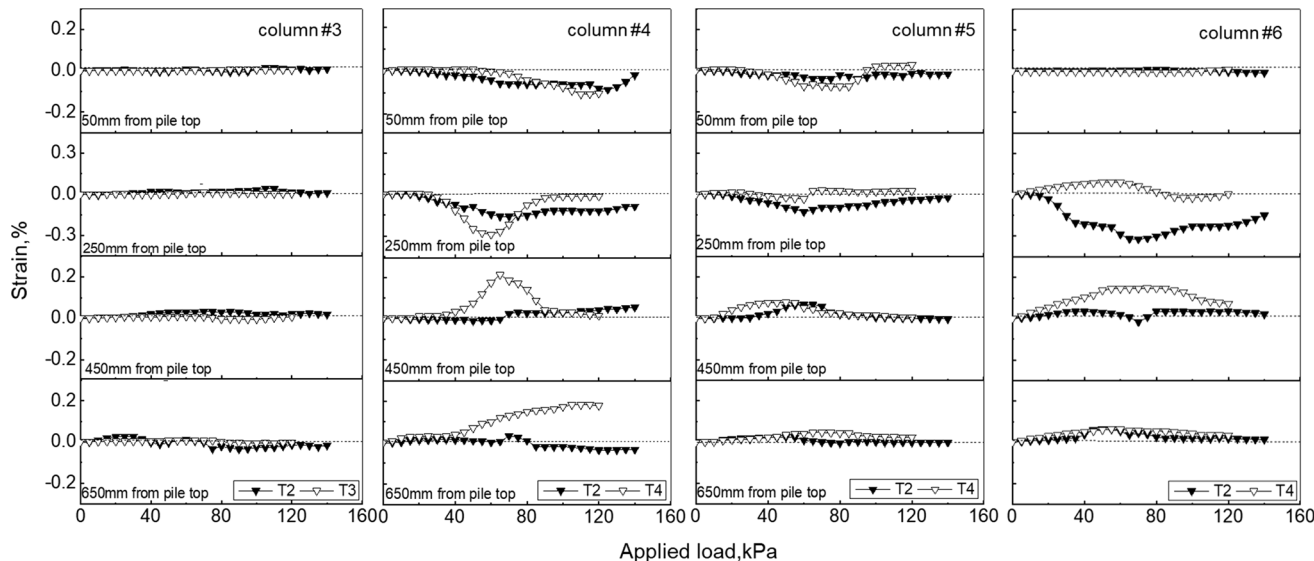
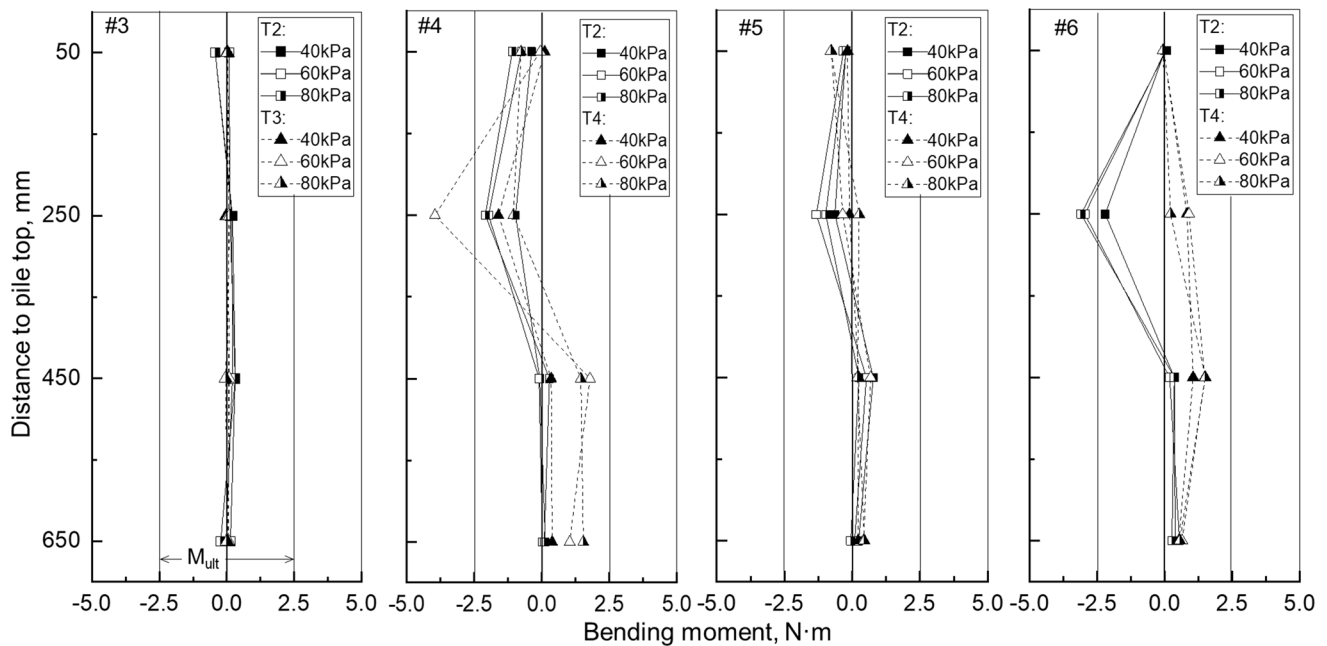


Fig. 8 Variation of column strain difference with the increase in applied load

Table 3 shows the applied surcharges when the LEDs for the columns #4 to #6 went out; however, the columns 1# to 3# are not included. As indicated previously, the columns 1# to 3# were mainly subjected to compression, but the aluminum foil tape was highly possible to be broken when the columns failed by bending. Therefore, the failure of the columns 1# to 3# may not be consistent with the moment for the LED going off. The columns failed progressively in order from the toe to the shoulder of the embankment. Meanwhile, the columns under the side slope of the embankment could fail under larger surcharge when there were columns under the embankment crest.

### 4.4 Failure modes of columns

After the test, the soft soil was excavated and the model columns were carefully removed from the model box. Figure 10 sequentially presents the model columns in each model tests in row R2. In the model test T2, the columns #1 and #2 nearly only had vertical deformation and the core pile penetrated upwards at the top of the column. Besides, some horizontal cracks and bulging of outer column were noticed. The column #3 was nearly integral, and it mainly had a vertical compression and inclination forwards. The columns #4 to #6 show large horizontal displacements, bending and multiple fractures.



**Fig. 9** The distribution of bending moment along core pile at different surcharge

**Table 3** The applied surcharge when the LED went out (unit: kPa)

Column No.	#4	#5	#6
T2	72	69	63
T4	66	60	56

In the model tests T3 and T4, similar to the corresponding column at the same position in the model test T2, the columns #1 to #3 mainly had vertical compression, and the columns #4 to #6 mainly had horizontal displacements and bending. However, there are still some differences from the test T2. The column #3 in the test T3 nearly had no horizontal displacement, and the failure mode of the column #5 and #6 in the test T4 were different from those in the test T2 in terms of fracture position and bending direction. The failure modes of the columns #5 and #6 agreed with their bending directions shown in Fig. 9.

Based on the above analyses, the columns under the embankment crest (columns #1 to #3) had possible failure under compression, the column under the embankment shoulder (column #4) had possible failure under a combination of compression and bending, and the columns near the toe of embankment (columns #5 and #6) had possible failure under bending. Yu et al. [22] also found that the failure mode of column was influenced by its position under the embankment when studying the rigid column-supported embankment, and pointed out that the failure modes of columns at different positions should be considered in design.

## 4.5 Slip plane of embankment

Based on the displacement contours of the embankment in the front side calculated by the Geo-PIV technique, the slip plane of the embankment can be determined. Figure 11 shows the slip planes in each test, and the column shapes after the embankment failure are illustrated as well. It can be seen that the existence of columns yielded a shallower slip plane than the test without columns; however, the slip planes did not exactly pass through the fracture positions on the columns. The slip plane in the test T4 was different from that in the test T2, although the slip plane only intersected with three columns under the side slope of the embankment. This is further indicated that the columns under the embankment crest could affect the stability of embankment.

## 5 Discussion on failure mechanism

### 5.1 Surcharges corresponding to the yielding or failure of columns

In engineering practice, limit equilibrium methods, such as Bishop's modified method and Spencer's three-part wedge method, have been commonly adopted to analyze slope stability of embankments over soft soils. They assume that the embankment fails along a slip plane (a circular slip plane or a three-part wedge failure plane) through soils and columns that provide shear strengths without considering the effects of the columns outside the slip plane. However,

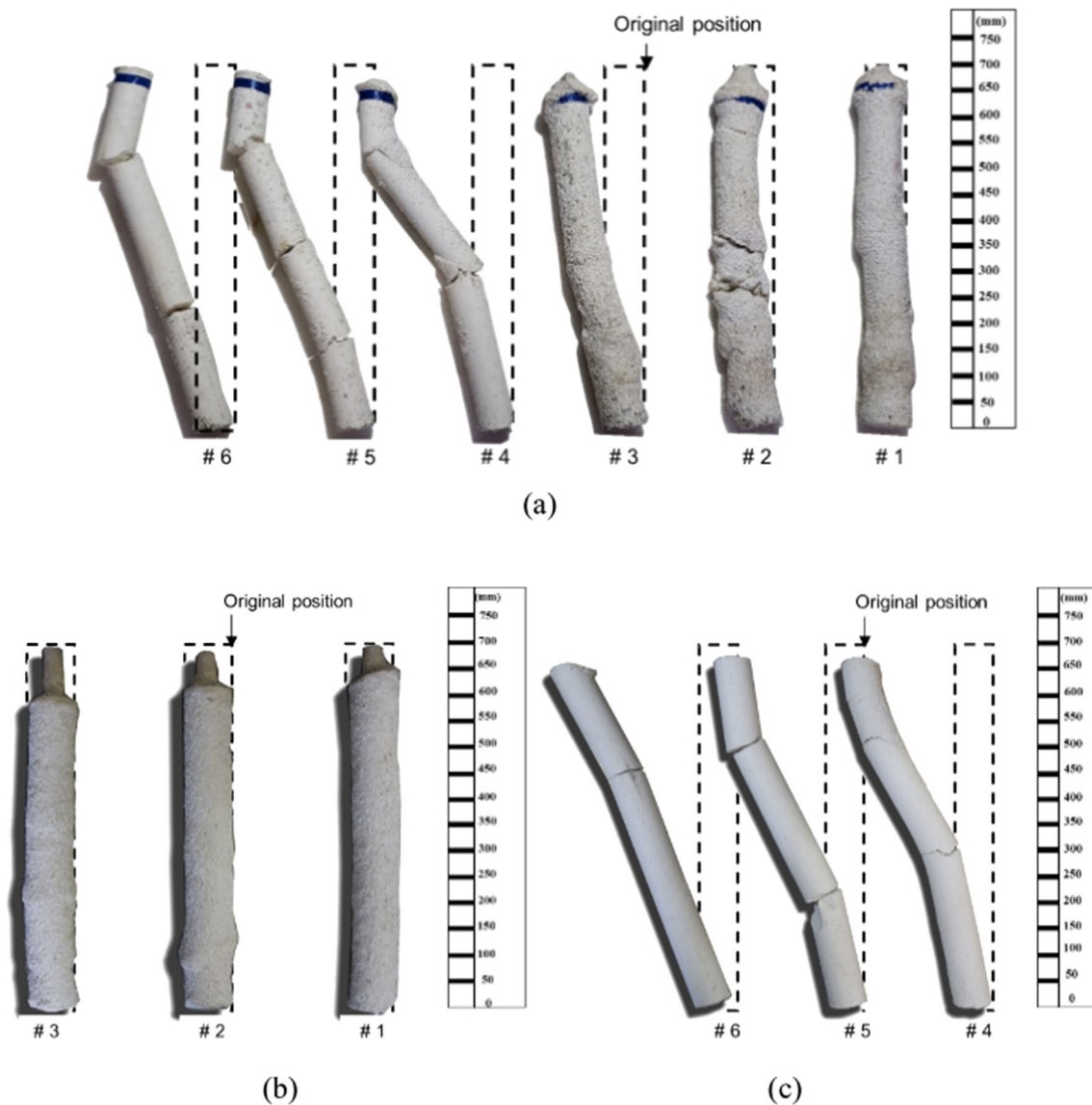


**Fig. 10** Failure modes of columns: **a** T2; **b** T3; **c** T4

this study revealed that the SDM column would not fail under shear, but they may fail under compression, a combination of compression and bending, and bending depending on their locations under embankment. The columns outside the slip plane had influence on enhancing the embankment stability.

In this study, the applied surcharges at special moments, such as the appearances of peak stress on the column head, the maximum strain difference along the core pile, and the LED going out, can be considered as the surcharge leading to the yielding or failure of the columns. Table 4 summarizes the applied surcharges corresponding to these special moments. As mentioned previously, the columns #1 to #3 had small strain differences at each depth, and their failure may not be consistent with the LED going off, thus only

the surcharges corresponding to the peak stress on the column head are listed. For the columns #4 to #6, the surcharges when the peak strain difference firstly appeared, and the LED went out are included.

The surcharges determined from the three conditions were not exactly consistent with each other. Generally speaking, the surcharges for the appearance of peak strain difference were the smallest and then, goes to the surcharges when LED went out, followed by the surcharge for the appearance of peak stress on the column head. The core pile failed lateral than the outer DM column. Additionally, the surcharges corresponding to the yielding and failure of the columns #1 to #3 were generally less than those in the columns #4 to #6.

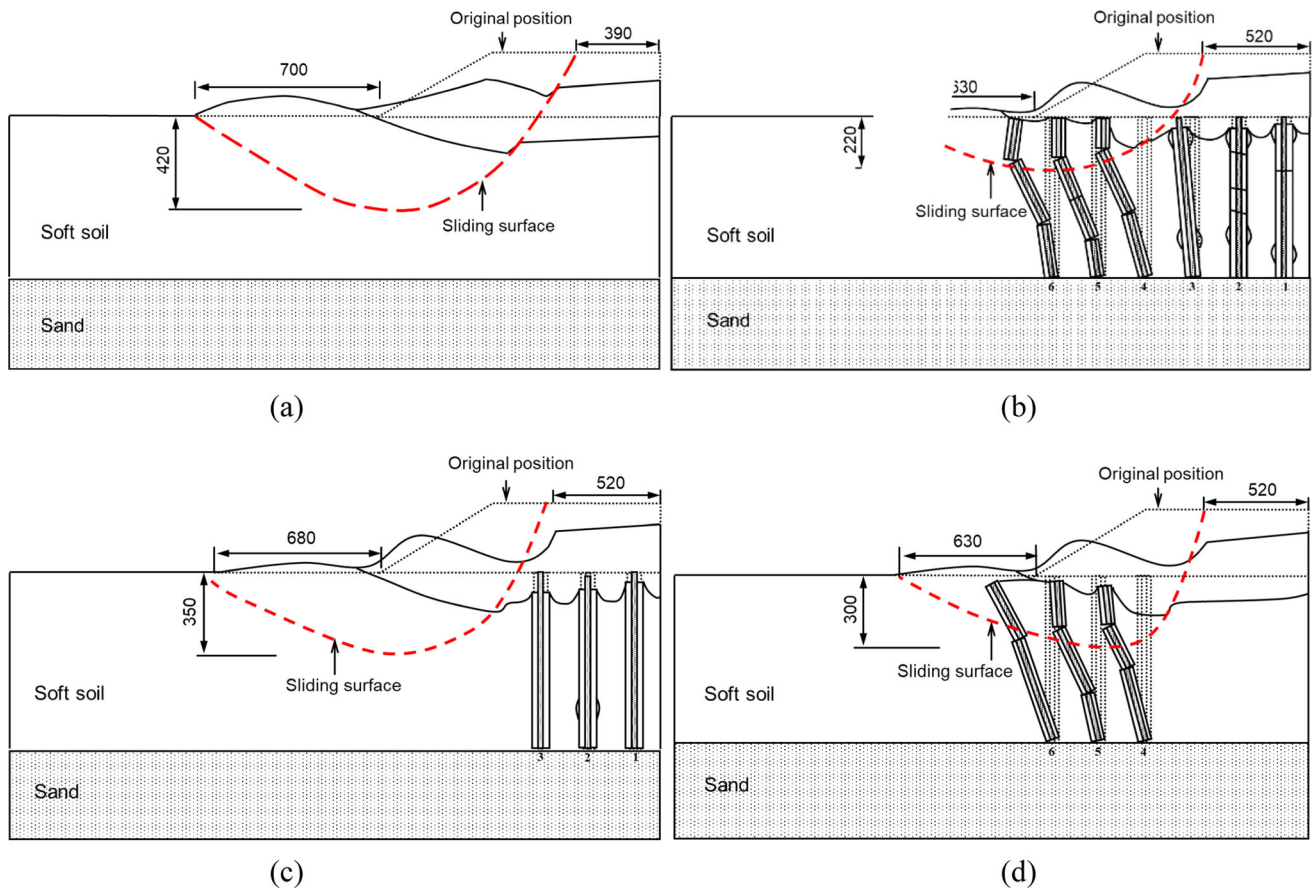


Fig. 11 Slip planes of SDM column-supported embankment: **a** T1; **b** T2; **c** T3; **d** T4 (unit: mm)

Table 4 The applied surcharges corresponding to the yielding and failure of columns

Model test	SDM column	#1	#2	#3	#4	#5	#6
T2	Core pile	–	62	55	85/72/65	–/69/60	–/63/50
	Outer column	38	60	48	58/–/–	–	–
T3	Core pile	60	65	70	–	–	–
	Outer column	50	50	35	–	–	–
T4	Core pile	–	–	–	70/66/58	–/60/40	–/56/50
	Outer column	–	–	–	55/–/–	–	–

Surcharges in columns #1 to #3 are those when peak stress on the column head appeared; and surcharges in columns #4 to #6 are in order of peak stress on the column head/ LED going out/ peak strain difference

### 5.2 Progressive failure of SDM columns

Based on the analyses and discussions in this study, the progressive failure mechanism of SDM columns could be revealed. The SDM column had larger stiffness than the soft soil, especially the core pile. Due to the load shearing effect, the columns #1 to #4 bore majority of the embankment surcharge. As a result, most additional stress induced by the surcharge was transmitted to the deep firm

soil layer through the SDM column. With the increase in the surcharge, the outer columns and core piles of the columns #1 to #3 successively yield and the additional stress were transferred back to the soft soil, leading to the surge of earth pressures in the soft soil. Such increase in the lateral earth pressure would cause the increase in the bending moment carried by the columns #4 to #6. Subsequently, the columns #4 to #6 progressively failed by bending. The column subjected to compression could carry

larger moment, thus the columns failed starting from the embankment toe. Figure 12 illustrates the progressive failure process. Zheng et al. [28] revealed the progressive failure mechanism of concrete columns under the embankment. However, the columns under the embankment toe failed by bending first, subsequently, the column under the embankment center gradually failed, leading to a global instability of the embankment. This could be explained by the fact that the concrete column had larger vertical bearing capacity than the SDM column.

In the model test T4, there were no columns under the embankment crest to share the surcharge. As a result, the lateral earth pressure in the soil increased significantly when small surcharge was applied. Such increase in lateral earth pressure led to the increase in bending moment in the columns #4 to #6. Therefore, the model test T4 failed at small surcharge as compared with the model test T2. The columns under the embankment crest contributes to enhancing the embankment stability although the slip plane

may not pass through them, as they reduce the growth rate of lateral earth pressure in soil.

It is worth mentioning that the SDM columns located under the side slope mainly bears bending moment. Thus, adopting a core pile with higher bending moment capacity for the SDM column under the side slope is beneficial to enhance the stability of embankment. Wonglert et al. [20] and Phutthananon et al. [16] found that SDCM column with wooden core pile can significantly improve the bending capacity of column. In addition, adding a lateral reinforcement can also enhance the bending behavior of columns. Yu et al. [23] presented that geosynthetics can significantly decrease the bending moment, making the columns less prone to bending failure. Ma et al. [13] found installing a ground beam to connect the piles under the side slope can reduce and equalize the bending moment distribution between piles.

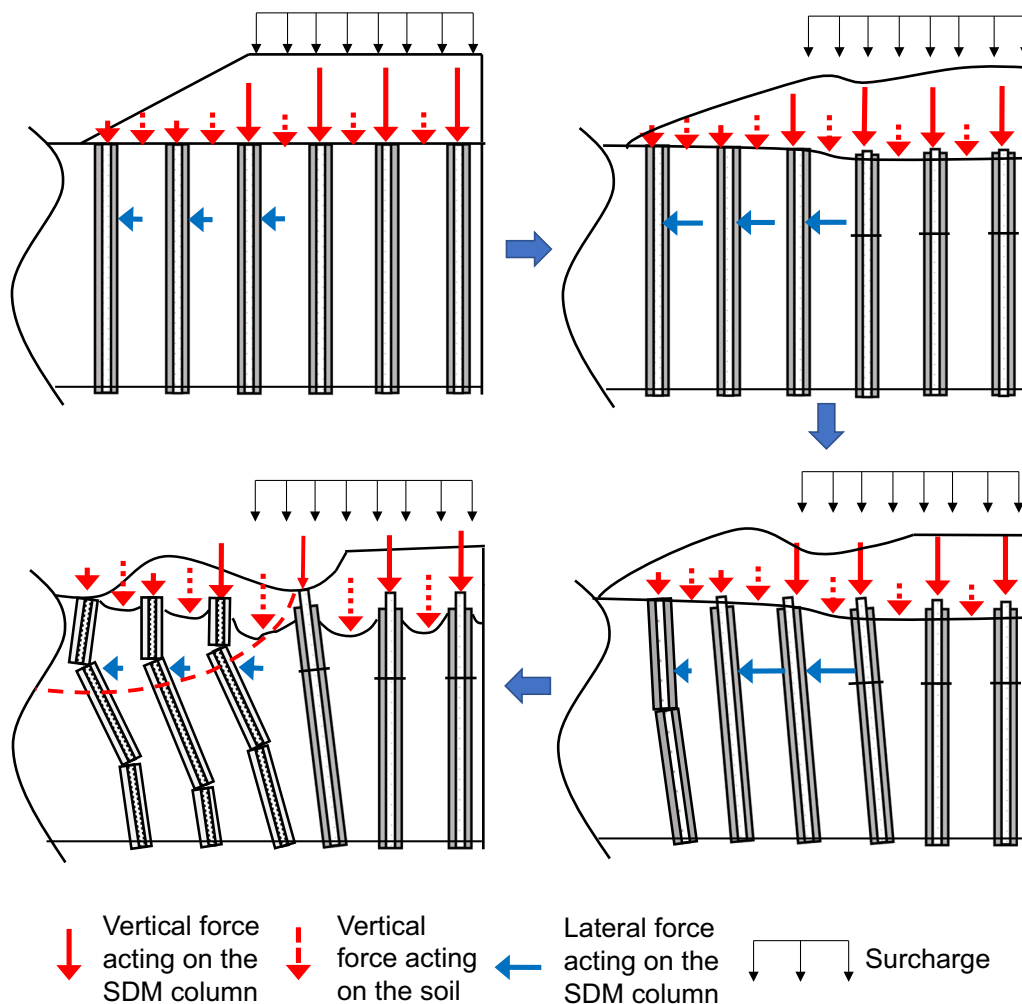


Fig. 12 The progressive failure process of SDM columns

## 6 Conclusions

This study conducted a series of scale-reduced model tests to investigate the stability of SDM column-supported embankment over soft soils. Based on the test results and discussions, the following conclusions can be drawn:

1. The embankment with SDM columns under the whole embankment base yielded higher stability as compared with that with SDM columns only under the side slope, even though the slip plane did not pass through the columns under the embankment crest.
2. The SDM columns under the embankment crest carried majority of the embankment surcharge due to the load shearing effect and transmitted the load to a deep firm sand soil, leading to reducing the bending moment on the columns under the side slope.
3. The failure mode of SDM column was influenced by its position. The SDM columns under the embankment crest had possible failure under compression, and the outer columns yielded earlier than the core pile. The column under the embankment shoulder had possible failure under a combination of compression and bending. The columns near the toe of embankment had possible failure under bending.
4. With the increase in surcharge, the SDM column failed progressively. The columns under the embankment crest successively yielded, leading to a surge of bending moments carried by the columns under the side slope. Subsequently, the columns under the side slope progressively failed by bending in order from the embankment toe to shoulder.

**Acknowledgements** The authors appreciate the financial supports provided by the Natural Science Foundation of China (NSFC) (Grant Nos. 41972272 & 41772281).

**Data availability statement** The data that support the findings of this study are available from the corresponding author, Guanbao Ye, upon reasonable request.

## References

1. Chai JC, Shrestha S, Hino T, Uchikoshi T (2017) Predicting bending failure of CDM columns under embankment loading. *Comput Geotech* 91:169–178
2. Chen JF, Liu JX, Ma J (2012) Calibration of a miniature cone penetrometer for geotechnical model test. *J Tongji Univ Nat Sci* 40(4):549–552 (in Chinese)
3. Dong P, Qin R, Chen Z (2004) Bearing capacity and settlement of concrete-cored DCM pile in soft ground. *Geotech Geol Eng* 22(1):105–119
4. Gao XN, Liu SY, Dong P (2012) Application of concrete-cored DCM pile in soft ground treatment of highway bridgehead. In: *Proceedings of the 4th international conference on grouting and deep mixing*, pp 261–271
5. Jamsawang P, Bergado DT, Bandari A, Voottipruex P (2008) Investigation and simulation of behavior of stiffened deep cement mixing (SDCM) piles. *Int J Geotech Eng* 2(3):229–246
6. Jamsawang P, Bergado DT, Voottipruex P (2011) Field behaviour of stiffened deep cement mixing piles. *Proc Inst Civ Eng Ground Improv* 164(1):33–49
7. Jamsawang P, Yoobanpot N, Thanasisathit N, Voottipruex P, Jongpradist J (2016) Three-dimensional numerical analysis of a DCM column-supported highway embankment. *Comput Geotech* 72:42–56
8. Jellali B, Bouassida M, de Buhan P (2011) Stability analysis of an embankment resting upon a column-reinforced soil. *Int J Numer Anal Meth Geomech* 35(11):1243–1256
9. Kivelo M, Broms BB (1999) Mechanical behaviour and shear resistance of lime/cement columns. In: *International conference on dry mix methods: dry mix methods for deep soil stabilization*, pp 193–200
10. Kitazume M, Maruyama K (2006) External stability of group column type deep mixing improved ground under embankment loading. *Soils Found* 46(3):323–340
11. Kitazume M, Maruyama K (2007) Internal stability of group column type deep mixing improved ground under embankment loading. *Soils Found* 47(3):437–455
12. Liyanapathirana DS, Yapage N (2021) A spreadsheet based stability calculation for geosynthetic reinforced column-supported embankments. *Transp Geotech* 29:100575
13. Ma HF, Luo Q, Wang TF, Jiang H, Lu QY (2021) Numerical stability analysis of piled embankments reinforced with ground beams. *Transp Geotech* 26:100427
14. Navin MP, Filz GM (2006) Numerical stability analyses of embankments supported on deep mixed columns. In: *Ground modification and seismic mitigation*, pp 1–8
15. Nguyen B, Takeyama T, Kitazume M (2016) Internal failure of deep mixing columns reinforced by a shallow stabilized soil beneath an embankment. *Int J Geosynth Ground Eng* 2(4):1–13
16. Phuthananon C, Jongpradist P, Wonglert A, Kandavorawong K, Sanboonsiri S, Jamsawang P (2023) Field and 3D Numerical Investigations of the Performances of Stiffened Deep Cement Mixing Column-Supported Embankments Built on Soft Soil. *Arab J Sci Eng* 48(4):5139–5169
17. Stanier SA, Blaber J, Take WA, White DJ (2015) Improved image-based deformation measurement for geotechnical applications. *Can Geotech J* 53(5):727–739
18. Voottipruex P, Bergado DT, Suksawat T, Jamsawang P, Cheang W (2011) Behavior and simulation of deep cement mixing (DCM) and stiffened deep cement mixing (SDCM) piles under full scale loading. *Soils Found* 51(2):307–320
19. Wonglert A, Jongpradist P (2015) Impact of reinforced core on performance and failure behavior of stiffened deep cement mixing piles. *Comput Geotech* 69:93–104
20. Wonglert A, Jongpradist P, Jamsawang P, Larsson S (2018) Bearing capacity and failure behaviors of floating stiffened deep cement mixing columns under axial load. *Soils Found* 58(2):446–461
21. Wang C, Xu YF, Dong P (2014) Working characteristics of concrete-cored deep cement mixing piles under embankments. *J Zhejiang Univ Sci A* 15(6):419–431
22. Yu JL, Zhou JJ, Gong XN, Xu RQ, Li JY, Xu SD (2021) Centrifuge study on behavior of rigid pile composite foundation under embankment in soft soil. *Acta Geotech* 16:1909–1921
23. Yu XX, Zheng G, Zhou HZ, Chai JC (2021) Influence of geosynthetic reinforcement on the progressive failure of rigid columns under an embankment load. *Acta Geotech* 16:3005–3012

24. Zhang Z, Rao FR, Ye GB (2020) Design method for calculating settlement of stiffened deep mixed column-supported embankment over soft clay. *Acta Geotech* 15(4):795–814
25. Zhang Z, Xiao Y, Ye GB, Han J, Wang M (2018) Numerical investigation on slope stability of deep mixed column-supported embankments over soft clay induced by strength reduction and load increase. In: *Proceedings of GeoShanghai international conference*, Springer, Singapore, pp 89–96
26. Zhang Z, Ye G, Cai YS, Zhang Z (2019) Centrifugal and numerical modeling of stiffened deep mixed column-supported embankment with slab over soft clay. *Can Geotech J* 56(10):1418–1432
27. Zheng G, Liu SY, Chen RP (2009) State of advancement of column-type reinforcement element and its application in China. In: *Proceedings of the 2009 US-China workshop on ground improvement technologies-advances in ground improvement: research to practice in the United States and China*, Orlando, Fla. Geotechnical Special Publication, GSP 188, pp 12–25
28. Zheng G, Yang X, Zhou H, Chai J (2019) Numerical modeling of progressive failure of rigid piles under embankment load. *Can Geotech J* 56(1):23–34
29. Zheng G, Yu X, Zhou H, Wang S, Zhao J, He X, Yang X (2020) Stability analysis of stone column-supported and geosynthetic-reinforced embankments on soft ground. *Geotext Geomembr* 48(3):349–356
30. Zheng G, Diao Y, Li S, Han J (2013) Stability failure modes of rigid column-supported embankments. In: *Geo-congress 2013: stability and performance of slopes and embankments III*, pp 1814–1817
31. Zhou HZ, Xu HJ, Yu XX, Guo ZY (2021) Evaluation of the bending failure of columns under an embankment loading. *Int J Geomech* 21(7):04021112
32. Zhao X, Wu M, Chen S, Kong D (2010) Study on bearing behaviors of single axially loaded SDCM pile. In: *Geotechnical special publication, Deep foundations and geotechnical in situ testing - proceedings of the 2010 GeoShanghai international conference*, 205 GSP, pp 277–284

**Publisher's Note** Springer Nature remains neutral with regard to jurisdictional claims in published maps and institutional affiliations.

Springer Nature or its licensor (e.g. a society or other partner) holds exclusive rights to this article under a publishing agreement with the author(s) or other rightsholder(s); author self-archiving of the accepted manuscript version of this article is solely governed by the terms of such publishing agreement and applicable law.